AIAA-2003-3496
Evaluation of a Monte Carlo Model for Two Phase Rarefied Flows

Jonathan M. Burt and Iain D. Boyd
University of Michigan
Ann Arbor, MI

36th AIAA Thermophysics Conference
23-26 June 2003
Orlando, Florida

EVALUATION OF A MONTE CARLO MODEL FOR TWO PHASE RAREFIED FLOWS

Jonathan M. Burt* and Iain D. Boyd†
Department of Aerospace Engineering
University of Michigan, Ann Arbor, MI 48109

ABSTRACT

A method proposed by Gallis et al. for the simulation of a dilute particle phase within a rarefied gas flow has been fully implemented in the Direct Simulation Monte Carlo code MONACO. The method is modified for use with a diatomic gas, and code validation is performed through comparison with published results of an experimental study on the aerodynamic focusing of a particle beam. Several simulations are run to reproduce the physical characteristics of these experiments, and a largely qualitative method is used to establish the accuracy of the simulations. Various particle properties are considered in the numerical results, and expected trends are observed.

INTRODUCTION

Two phase flows consisting of solid particles suspended in a carrier gas are commonly found in aerospace applications, and accurate analysis and prediction of particle properties is often crucial to an understanding of the net flow characteristics. Numerous experimental and numerical studies have examined a broad range of two phase flow regimes, and several existing CFD programs[1,2] allow accurate modeling of complex multiphase flows in almost any case where quasi-equilibrium and continuum flow assumptions can be made for the carrier phase. However, few studies have been devoted to rarefied two phase flows, where the nonequilibrium nature of the gas prevents traditional CFD calculations from yielding accurate results, and where experimental studies may be prohibitively expensive due to the requirements on test facilities and instrumentation.

The modeling of rarefied two phase flows is of particular interest in the design and analysis of high-altitude rocket propulsion systems. Alumina particles ejected from solid-propellant rocket motors may account for a large portion of the mass flow rate through the nozzle, and radiation from these particles is the dominant contributor to the plume emission signature. In exhaust plumes for liquid-propellant rockets, soot particles and agglomerates may contribute significantly to the emission signature, and particle velocity lag through the nozzle will reduce nozzle efficiency. Particle impingement on nozzle walls may lead to surface erosion and a further loss of efficiency, and momentum or energy transfer between the particles and gas can affect gas properties in both the nozzle and plume. In addition, solid particles or clusters ejected from satellite thrusters may impinge on and contaminate fragile satellite components. The existence of a computational method for modeling such flows therefore has great potential as an aide in the design and analysis of both rocket propulsion systems and satellite thrusters.

This paper describes the implementation of a recently developed numerical model for the particle phase in a rarefied particle-gas flow. The relevant algorithms for this model are added to an existing code which uses a kinetic theory-based representation of the constituent molecules in a gas, and is capable of accurately simulating highly rarefied or nonequilibrium gas flows. As modified for the simulation of two phase flows, the code should then allow for accurate modeling of the solid particle phase in high altitude rocket exhaust or spacecraft thruster plumes. The accuracy of the numerical method is assessed through the comparison of simulation results with experimental data on the aerodynamic focusing of a solid particle beam. Additional simulation results are presented, and arguments are provided for the validity of observed trends. Finally, the overall accuracy of the interphase heat transfer formulation is evaluated by observing expected trends in other simulation results. Several additions and modifications to the code are required for consideration of all of the flow characteristics and physical processes discussed above, and major planned and ongoing modifications are described.

NUMERICAL MODEL

The Direct Simulation Monte Carlo (DSMC) method[3] has in recent years become a standard tool for analyzing rarefied gas flows, and although far more computationally expensive than traditional CFD methods, it allows relatively efficient modeling of flows for which all standard CFD codes fail. One such flow is the free expansion of a gas into a vacuum, as occurs in high-altitude rocket exhaust or satellite thruster plumes. The DSMC method is therefore an ideal foundation for the simulation of the two phase free expansion flows of interest. In a recent paper by Gallis et al.[4], equations are

* Graduate student, AIAA student member.
† Professor, AIAA associate fellow.

derived for the average force and heat transfer rates to a small spherical solid particle moving through a gas with a delta-function incident velocity distribution. These equations can be used as the basis for the inclusion of solid particles in a DSMC code, and therefore as a starting point for a general method of simulating two phase rarefied flows.

Through the use of these equations, the existing DSMC code MONACO[5] has been modified to allow for the creation, tracking, and cell-averaged property calculations of a solid particle phase within a two dimensional or axisymmetric gas simulation. The particles are assumed to be chemically inert, spherical, and small enough so that each particle is only influenced by gas molecules located in the same grid cell as the particle center. A low Biot number approximation is used, as the temperature is assumed to be spatially uniform within each particle. Following standard practice for the particle size distribution, particle diameters are given either a truncated Gaussian or log-normal distribution[6], with the potential for implementation of additional distributions as needed. Particle-particle collisions and interphase mass transfer are not considered, and an assumption is made of one-way coupled flow: The gas phase momentum and energy flux are assumed to be much greater than the momentum and energy transfer rates respectively from the particles to the gas, so that the two latter quantities can be neglected.

A Lagrangian particle representation is used, where each computational particle tracked through the simulation represents multiple solid particles in the actual flow being modeled. The method of Chen[7] is employed for tracking particle center locations through an arbitrary unstructured grid, and particle movement – as with gas molecule movement – is decoupled from the momentum and energy transfer to the particles during each time step. A wall-impact model[6] based on two-body impulse equations is included, allowing for both finite particle-wall interaction periods and surface deposition, while neglecting any post-collision angular momentum of the particles. As is the case in virtually all two phase free expansions of interest, the particle mass is assumed to be much greater than the mass of the gas molecules, so that Brownian motion of the particles can be ignored without much loss of accuracy.

As described by Gallis et al.[4], the average rates of momentum and energy transfer to a solid particle from a computational gas molecule within the same grid cell can be calculated by considering the computational gas molecule as a large spatially homogeneous collection of individual gas molecules, which move through the cell at a uniform incident velocity. A fraction of these molecules will collide with the particle during a given time step, and those that do collide will be deflected off the particle surface in one of three ways: either by specular reflection, by isothermal diffuse reflection with full accommodation to the particle temperature, or by adiabatic diffuse reflection where the molecule speed relative to the particle is unchanged in the collision. As previous analysis of experimental data[8] has shown that gas-solid interactions in rarefied flow can be accurately modeled as involving only the first two types of reflection, adiabatic diffuse reflection is not considered in the current implementation of the method While these equations are intended for use in a DSMC simulation involving a monatomic gas, the code allows for consideration of diatomic gases by assuming that in a gas-solid collision involving isothermal diffuse reflection, the translational, rotational and vibrational energy modes of the gas molecule are all fully accommodated to the particle temperature.

Given these assumptions and modifications, the energy transfer rate to a solid particle due to the presence of a computational gas molecule within the same grid cell is calculated using the following expression:

$$\dot{Q}_p = \frac{\pi R_p^2 \tau N_g c_r}{V_c}\left(\frac{1}{2}mc_r^2 + e_{int} - (2+\sigma)k_B T_p - \frac{k_B \theta_v \sigma}{\exp(\theta_v/T_p)-1}\right) \quad (1)$$

Here R_p is the radius of the solid particle, V_c is the cell volume, τ is the thermal accommodation coefficient for the particle, N_g is the gas molecule relative weight (the number of real molecules represented by each computational gas molecule), c_r is the relative speed of the computational molecule with respect to the particle, m is the mass of an individual gas molecule, and e_{int} is the total internal energy (including rotational and vibrational modes) of the computational molecule. Additionally, k_B is Boltzmann's constant, T_p is the particle temperature, θ_v is the characteristic temperature of vibration for the gas species, and σ is a dimensionless parameter set to equal one for a diatomic gas or zero for a monatomic gas. Under the assumption that the vast majority of the energy lost by a gas molecule during the collision process is transferred to the particle as thermal energy, Equation 1 can be used to compute the rate of heat transfer to the particle. The corresponding force on the particle can be given as

$$\mathbf{F}_p = \frac{\pi R_p^2 N_g}{V_c}\left(mc_r + \frac{\tau}{3}\sqrt{2\pi m\, k_B T_p}\right)\mathbf{u}_r \quad (2)$$

where $\mathbf{u}_r$ is the relative velocity of the gas molecule with respect to the particle.

Note that the thermal accommodation coefficient τ is equal to the fraction of interphase collisions which involve diffuse reflection, and that the remaining fraction $(1-\tau)$ of collisions involve specular reflection. Also note that no consideration is made for the effect of collisions between reflected molecules and incident molecules surrounding the particle, so that the

gas is assumed to be locally free molecular for the calculation of gas-particle interactions. As a result, this method neglects the significant variation in the gas velocity distribution over the particle surface expected in low particle Knudsen number flow. In fact, a detailed comparison with existing numerical data and empirical correlations[9] has shown the method to develop significant inaccuracy for particle Knudsen numbers below around three. It should be remarked, however, that this comparison only considers the single set of flow conditions listed in Reference 9, and that under different conditions the method may retain a high degree of accuracy well into the slip flow regime.

As implemented in the code, the temperature and velocity of a particle are updated during each time step by summing over the force and heat transfer contributions of every computational gas molecule within the same grid cell, using Equations 1 and 2. The resulting change in particle temperature is then calculated as the total heat transfer rate multiplied by a factor $\Delta t/(M_p c_s)$, where Δt is the size of the time step, M_p is the particle mass, and c_s is the specific heat of the particle. Likewise, the change in particle velocity is equal to the total force multiplied by $\Delta t/M_p$.

COMPARISON WITH EXPERIMENT

Initial code validation is performed through comparison with the results of an experimental study by Israel and Friedlander[10], which examines the aerodynamic focusing of aerosol beams exhausting into a vacuum. As described by the authors, a particle-air mixture is ejected through a convergent nozzle into a near vacuum, with a small plate oriented normal to the nozzle axis placed some distance downstream. In the near-field free expansion region just beyond the nozzle exit, the gas and particles interact in such a way that the particle trajectories, and therefore the size of the particle beam, will depend on the source pressure p_o of the gas. The solid angle δ of the beam is determined by measuring the area of the particle deposition on the plate.

As discovered by Israel and Friedlander, there is a particular source pressure, or range of pressures, for which the value of δ is minimized. This is explained by the following logic: As the gas freely expands in the region just beyond the nozzle exit, a force is exerted on the particles in the outward radial direction, following the streamlines of the gas. This outward force counters the initially inward-directed momentum of the particles as they tend, due to inertia, to follow straight trajectories after exiting through the convergent nozzle. At relatively high values of p_o, the influence of the gas outweighs the influence of particle inertia, so that the particles are redirected by the gas into outward radial trajectories, and the particle-gas interaction acts to increase the value of δ. Likewise, at very low source pressures, the gas exerts little influence on the particles in the near-field expansion region, and the particles tend to follow relatively straight trajectories that pass through the central axis, then continue in radially outward directions further downstream. Thus, at some intermediate p_o value, the countering influences of drag and particle inertia will cancel each other out. Particle trajectories will then be nearly parallel to the nozzle axis in the far-field plume region, and the size of the particle beam will be minimized.

Experiments were conducted by Israel and Friedlander over a wide range of source pressures, using three different sizes of spherical latex particles. As the largest particles were found to have Knudsen numbers too small for accurate modeling using the equations discussed above, and as particle depositions corresponding to the smallest particle size were found in the experiment to show a less conclusive trend, only the medium-sized particles – of diameter 0.365 μm – are considered in the simulations used for comparison with experimental results. While these experiments only allow for direct validation of the Gallis momentum transfer formulation as implemented in the current code, the existence of a source pressure for which the beam size is minimized – as well as agreement in the value of this pressure – can provide convincing evidence of the overall accuracy and functionality of the code.

Due to both the enormous computational expense of DSMC simulations involving regions of relatively high density gas, and the fact that the DSMC method often requires massive computation time to produce accurate flow rates in simulations involving very low Mach numbers, the grid domain in all simulations described here includes only the comparatively high Mach number ($M \geq 0.2$), low density section of the nozzle within 1mm of the throat. Following the description of nozzle geometry in the experimental paper, the inflow boundary then corresponds to a local nozzle radius of 0.2352 mm, with a specularly reflecting wall converging at a constant angle of 3.25 degrees toward a throat of radius 0.0785 mm. Additional boundary conditions imposed in the simulations include a specularly reflecting wall along the plane of the nozzle exit, outflow boundaries parallel and normal to the central axis which runs through the nozzle, and a symmetry boundary along this axis.

Although gas properties within the nozzle could, in theory, be more accurately modeled through the use of diffusely reflecting – rather than specular – wall boundaries, the resulting boundary layer along the nozzle wall would be very thin relative to the size of the grid. As large gas property gradients are expected within this boundary layer, accurate simulation would require a reduction in cell size along the nozzle wall, and the computational expensive of each simulation

would increase considerably. Moreover, it can be assumed that the existence of a thin boundary layer along the nozzle wall would have little if any influence on particle properties in the far-field region of the plume.

Not counting the region within the nozzle, the grid used in all simulations extends an axial distance of 6mm and a radial distance of 0.8 mm, comprising a total of about 31,600 cells. As described in the experimental paper, a skimmer is used to aid in evacuating the gas in the region just beyond the nozzle exit, while not interfering with particle trajectories in the beam. Because insufficient details are given of the skimmer geometry, it is neglected in the boundary conditions of the simulations described here. Moreover, the skimmer is used in the experiments only to better facilitate the desired far-field vacuum condition, so it should not in principle need to be considered in simulations where this condition can be prescribed through the use of outflow boundaries.

For all cases considered, the source temperature is 298 K, and assumptions of one-dimensional isentropic flow within the nozzle give an inflow Mach number of 0.20, with a corresponding static temperature of 295.63 K and axial gas velocity of 69.176 m/s. Note that all of these values are independent of the source pressure. The inflow static pressure is determined using the isentropic relation between the inflow and source temperatures and pressures. The gas number density along the inflow boundary is then calculated from the inflow temperature and pressure, using the ideal gas law. For simplicity, and with likely little influence on the simulation results, the inflow gas radial velocity is set to zero. Following an assumption that the particles experience very little temperature variation through the low Mach number section of the nozzle not included in the grid domain, the inflow particle temperature is set to equal the source temperature of 298 K. Further, the inflow axial particle velocity is assumed to equal that of the gas, and the corresponding particle radial velocity is calculated such that, within the plane of symmetry defined by the grid, all particle velocity vectors along the inflow boundary are parallel to the wall.

This last approximation, while greatly oversimplifying the particle trajectories at the inflow boundary, can be assumed to allow for accurate representation of the particle properties within the plume. As evidence of the validity of this assumption, consider the following two cases: First, when the source pressure is relatively high, the particles tend to follow the gas streamlines throughout the nozzle, so that any significant difference between the local gas and particle radial velocity components at the inflow boundary will quickly disappear a short distance downstream. Second, if the source pressure is very low, then the particles will not follow the streamlines within the nozzle, and particles will tend to impact the walls and pass through the central axis in a manner that seems physically consistent with the inflow condition described here. For comparison, a few simulations are repeated using values of the particle inflow radial velocity component that scale with distance from the central axis, such that particle trajectories along the inflow boundary are parallel to the nozzle wall only at the point where the inflow and wall boundaries meet. As described below, these simulations result in very small beam sizes for low source pressures, as the lack of particle-wall collisions allows for a very small "focal point" of the beam, some distance downstream of the nozzle, where the beam diameter approaches zero as the source pressure is reduced. While focal points were observed in the experiments involving the largest particle size (which is not considered here) the lack of particle-wall collisions, and the assumption that particles follow the gas streamlines even for very low source pressures, does not reflect the expected physical characteristics of the flow, and the results from these simulations can be considered less valid than those for which the inflow particle velocity is constant.

In all simulations, the gas is a mixture of N_2 and O_2 with mass fractions of 0.79 and 0.21 respectively, as used in the inflow conditions of Reference 9. Axisymmetric simulations have been performed over a range of source pressures p_o from 14.8 mmHg to 96 mmHg, each corresponding to a p_o value used in the experiment. The gas molecule relative weight N_g varies from 3×10^8 to 6×10^8 depending on the source pressure, so that approximately 200,000 computational gas molecules are simultaneously tracked through the grid. For all cases considered, the analogous relative weight N_p of the particle phase is set to equal one, and the inflow particle mass flux m_p is 0.12 kg/m^{2}s. This corresponds to a particle number density of about 6.1×10^{13} particles/m^3 along the inflow boundary, and a total of between 10,000 and 15,000 particles simultaneously within the grid domain. Following experimentally determined properties for latex or similar materials, all particles are given a specific heat of 2180 J/kg K, a material density of 1120 kg/m^3, and a thermal accommodation coefficient of 0.89.

Note that collisions between particles, as well as the effect of interphase collisions on the gas, are not considered, so that the magnitude of m_p will have no influence on any flow properties other than the particle fluxes and bulk densities. Of the properties which are affected, all trends (for example, the shape of iso-contour lines) will still be independent of the value of m_p. As no values for particle flux or flow rate are given by Israel and Friedlander, the value of 0.12 kg/m^{2}s used here is chosen only so that the number of particles

tracked through the grid is large enough to allow for relatively low statistical scatter, but not so large that excessive computational expense is required for convergence to steady state.

Flow properties in each cell are averaged over approximately 300,000 time steps following convergence. Figure 1 is included here for clarification of the grid geometry and basic flow field characteristics, and shows the Mach number of the gas at an intermediate source pressure of 34.5 mmHg. For all simulations, the particle number flux along the planar outflow boundary is plotted in Fig. 2 as a function of distance r from the axis.

Ideally, the profiles shown in Fig. 2 would have relatively flat regions near the central axis, followed in each case by a sharp drop-off to zero at a radial value r_o that could be interpreted as the "edge" of the particle beam. The corresponding beam solid angle could then be calculated as $\delta = \pi r_o^2/L^2$ where L = 6 mm. Unfortunately, as displayed in the figure, the radial decay in the number flux is approximately exponential, particularly for the lower source pressures considered. While the edge of a particle beam could therefore be defined as the r value for which the number flux drops below some given value, the resulting δ values would then be highly dependent on both the cutoff value chosen and the assumption that, in all experiments for which the simulation results are to be compared, the particle deposition was collected over approximately the same time interval.

A more characteristic value to use for the radial length scale – if not the beam radius itself – would be one that describes the size of the highest flux region near the axis, as well as the dependence of the observed deposition size on the time interval over which the deposition was collected. A smaller length scale, and therefore a smaller δ value, would then correspond to a weaker dependence of the deposition size on the time interval, so that running the experiment for longer would do little to increase the deposition size. Based on the observation that the outflow particle number flux scales roughly exponentially with r for most source pressures considered, the following radial length scale is used: For each set value of the source pressure p_o, $f(r) = B \exp(-Ar)$ is the exponential trend line for the outflow particle number flux profile, where A and B are constants determined from a least-squares fit. A larger value of A then corresponds to a number flux distribution more closely concentrated toward the central axis. Thus, by dimensional reasoning, the particle deposition radius r_o should scale roughly with 1/A, which can then be used as the relevant length. Finally, as the solid angle δ is proportional to r_o^2, it follows that δ should scale with $1/A^2$. The simulation results shown in Fig. 2 are used to obtain A values corresponding to each source pressure p_o considered, so that the variation of δ with p_o can be approximated from the simulations and compared to analogous experimental results.

Note that, in addition to the simplifying assumptions used to define the boundary conditions and other simulation parameters, a major potential problem with this validation method is that values of A will depend on the radial distance over which the least-squares trend line fit is performed, as well as the distribution of grid points along the outflow boundary. This dependence is particularly large at higher source pressures, where the outflow number flux distribution is shown in Fig. 2 to vary significantly from an exponential shape. For consistency, all A values are calculated using exponential trend lines that extend over the entire radial distance for which the outflow particle number flux is nonzero. It can be argued that equally valid but very different values of A could be found by performing each least-squares fit over a different set of grid points, or by neglecting the points where the particle number flux is nearly zero. Subject to these inherent problems and simplifications, it is still expected that, if the simulations accurately model the flows considered in the experiments, the plot of p_o against $1/A^2$ from the simulation results will have the same general shape as a plot of p_o against δ from the experiments.

Figures 3 and 4 show, respectively, the dependence of $1/A^2$ on p_o from the simulations, and experimental values of δ as a function of p_o. A comparison of the trends on the two plots reveals some major differences: The sharp increase in beam size at very low source pressures, as found in the experiment, is far less pronounced in the numerical results. The range of p_o values for which the beam size varies little with p_o is much smaller in Fig. 3 than in Fig. 4, where this range extends from p_o = 34.5 mmHg through 96 mmHg, the largest source pressure considered in the simulations. However, two very important trends are found in both plots. First, in both figures, there is a reduction in beam size as p_o is increased from the lowest value (14.8 mmHg), with a consistently positive curvature that leads to a minimum beam size, followed by an increase in beam size with source pressure as p_o is further increased. Second, the p_o value for which the beam size is minimized is the same (34.5 mmHg) in both figures. Furthermore, the comparatively rapid increase in beam size with p_o observed on the right side of Fig. 3 can be attributed to the fact that, for the corresponding simulations, the outflow number flux profiles are not very well correlated with the exponential trend lines used to define the beam size.

Note the data points in Fig. 3 marked with "+" symbols, which correspond to the simulations for which the radial component of particle velocity along the inflow boundary is set to vary with distance from the

axis. As discussed above, these simulations should under-predict the beam size for lower source pressures, so that the trend observed in figure 3 of a monotonic increase in beam size with p_o should not be thought to reflect the overall accuracy of the simulation method.

Figure 5 shows the dependence on p_o of the average terminal particle velocity $u_{p\infty}$ along the central axis, as measured from the simulation results at the outflow boundary 6 mm downstream from the nozzle exit plane. Because a denser gas exerts greater force on the particles as it expands within and beyond the nozzle, the trend of increasing $u_{p\infty}$ with p_o observed in the figure is very much expected. Experimental measurements of $u_{p\infty}$ give values of roughly 200 m/s for source pressures of both 34.5 mmHg and 65 mmHg, subject to errors of approximately 10 m/s. While the difference between experimental and simulation results is significant here, it should be noted that the terminal bulk gas velocity along the axis is found numerically to exceed 700 m/s, so that, as a fraction of the terminal gas speed, the differences in particle speed are relatively small.

Subject to the assumptions and simplifications described above, the simulation results agree well with data from the experiments. In general then, it can be assumed that both the two phase DSMC method of Gallis et al. and the current implementation of this method do function as expected, and allow for relatively accurate simulation of two phase rarefied flows. Note however that only dilute particle concentrations have been considered, as the Gallis method only allows for simulations of one-way coupled flow where the influence of the particle phase on the gas can be neglected. While not explicitly stated by Israel and Friedlander[10], it is assumed that the particle concentrations in the experiments are small enough so that the rate of momentum transfer from the gas to the particles is consistently much smaller than the gas momentum flux, so that any two-way coupling effects are negligible and the Gallis method can be used in simulating these flows. As discussed in the introduction, the assumption of one-way coupling is not always valid for the two phase plume flows of interest, where interphase momentum and energy transfer may significantly alter the properties of the gas. A detailed numerical model for two-way coupling is therefore under development. The derivation, implementation, and validation of this model will be discussed in a future paper.[11]

FURTHER NUMERICAL RESULTS

As the simulations described here are likely the first for which the DSMC-based approach of Gallis et al. is used to model two phase rarefied free expansion flows, additional simulation results of interest are provided. These results, although not usable for comparison with the experiments, demonstrate the utility of the method and the large variety of output information which may be obtained from the simulations, while allowing for a deeper understanding of the physical characteristics of the flows considered here. In Fig. 6, magnitudes of average particle (top) and gas (bottom) velocity are shown for the simulation corresponding to a source pressure of 34.5 mmHg, for which the particle beam size is minimized. Note the well-defined edge of the particle beam. As expected, the particles reach an approximate terminal velocity within a very short distance of the nozzle exit. Throughout the far-field region, the gas speed is far greater than the average particle speed, yet the gas density is too small for the gas to significantly accelerate the particles. The far-field reduction in gas density can be observed in Fig. 7, which shows the particle and gas number densities for the same simulation.

An interesting trend observed in Fig. 7 is that throughout the domain of the particle beam, the gradient in the gas number density is roughly orthogonal to the particle number density gradient. The reasons behind this relation can be traced to the well documented gas density variation in a freely expanding plume[12], and to the above analysis of particle number flux profiles.

Average particle temperature and gas translational temperature are shown in Fig. 8, again for the 34.5 mmHg simulation. The significant statistical scatter observed in both plots is primarily a consequence of the small separation between some neighboring contour levels, as is required to display the variation in particle and gas temperatures throughout both the nozzle and plume. To reduce the scatter, averaging has been performed over approximately 1.3 million time steps, which is more than four times the number used in the other simulations, so should allow for roughly twice the level of convergence. Note that there is negligible variation in particle temperature throughout the plume, and that even within the nozzle, the particle temperature varies by only a few degrees.

Figure 9 shows the variation in the relative Mach number M_p of the particles with respect to the surrounding gas. M_p is defined here as the magnitude of the vector difference between the cell-averaged velocities of the particles and the gas molecules, divided by the local sonic speed of the gas. Values of M_p are plotted along the central axis for simulations at source pressures of 14.8, 34.5 and 96 mmHg. The first and last of these pressures are, respectively, the lowest and highest p_o values considered in this study. The inclusion of results from these three simulations should therefore allow for an understanding of the full range of flow conditions. Note that points with x-coordinate

values between 0 and 0.001 m are located within the nozzle, and all other points are in the plume.

Neglecting the significant but expected statistical scatter in the far-field region of the plume, in all three simulations the relative Mach number is found to continuously increase with downstream distance. This follows from the fact that throughout both the nozzle and plume, the gas velocity is increasing and the gas temperature is decreasing, while the particle velocity varies far less rapidly. To reinforce this last point, a corresponding plot of average particle speed along the central axis is included here as Fig. 10.

As discussed above in the comparison with experimental results, the particles are shown in Fig. 10 to reach a near-terminal velocity within a short distance of the nozzle exit, and the magnitude of this terminal velocity increases with the source pressure p_o. An interesting trend observed in Fig. 10 is that the size of the near-field region of the plume where particle acceleration is significant has little, if any, dependence on the value of p_o.

Figure 11 shows the magnitude of the average drag force $\mathbf{F}_p$ on the particles along the axis. This force is equal to the dot product of the particle velocity and the spatial particle velocity gradient, multiplied by the particle mass. Thus, $|\mathbf{F}_p|$ can be thought to scale roughly with the slope of the particle speed curves plotted in Fig. 10. A comparison with Fig. 11 then explains the general trends observed in Fig. 10, most notably that the lack of variation in far-field particle velocity corresponds to a sharp drop-off in the force exerted on the particles by the expanding gas.

Another prominent trend in Fig. 11 is that for all three simulations considered, the values of $|\mathbf{F}_p|$ are far greatest around the nozzle exit, with a global maximum at the exit plane. This can be explained by the following logic: At the inflow boundary, the average particle and gas velocities are approximately equal. Thus, even though the gas density is greatest at this boundary, the drag force should be relatively small. (It is thought that the thermophoretic force due to the gas temperature gradient is significant here, and accounts for the fact that $\mathbf{F}_p$ is still much greater at the inflow boundary than in the far-field region of the plume.) As the gas expands and accelerates through the nozzle, the particle velocity lag dramatically increases, and as a result, $|\mathbf{F}_p|$ values increase greatly with downstream distance through the nozzle. The particle velocity lag continues to grow as the gas expands beyond the nozzle exit, but there is a rapid reduction in gas density that offsets the increasing relative velocity of the gas. Values of $|\mathbf{F}_p|$ will therefore decrease throughout the plume. The force exerted on the particles is then maximized at the nozzle exit, where the slope of the $|\mathbf{F}_p|$ profile changes sign. Furthermore, the requirement that $|\mathbf{F}_p|$ values be relatively small within a short distance both upstream and downstream of the nozzle exit gives rise to a sharp spike in the force profile at the exit plane, as shown in the figure.

The variation in particle Knudsen number along the central axis is displayed in Fig. 12. For all three simulations, the particles are found to be in the transition regime within and just beyond the nozzle, and well within the free molecule regime further downstream. The trend observed of rapidly increasing particle Knudsen number in the plume is reflected in Fig. 7, where the gas number density for the 34.5 mmHg simulation is shown to decrease greatly with downstream distance through the plume. Note the distinction between the particle Knudsen number, which characterizes the effect of collisions in creating local variation in the gas properties near the particle surface, and the Knudsen number of the flow, which characterizes the overall influence of collisions on average properties in the gas.

As mentioned above, all simulations used for comparison with experimental results are characterized by a lack of significant energy transfer between the particles and gas. This is reflected in Fig. 8, where the particle temperature is shown to be nearly uniform throughout the grid. In order then to consider the effects of interphase energy transfer, the simulation boundary conditions must be changed in ways that do not reflect the flow characteristics in the experiments. As the particle temperature is almost universally greater than the local gas temperature in the two phase plume flows discussed in the introduction, a simple and desirable way to evaluate the heat transfer formulation is to perform simulations where the particle temperature at the inflow boundary is much greater than the local temperature of the gas, and where all other parameters are unchanged from the simulations described above. Thus, the simulations corresponding to source pressures of 14.8, 34.5, and 96 mmHg are repeated with the inflow particle temperature increased by 100 K to 398 K.

Figure 13 shows the variation in the magnitude of the interphase energy transfer rate along the central axis, for all three of these simulations. While the temperature difference between the gas and particles is found to increase continuously with downstream distance in both the nozzle and plume, the heat transfer rate from the particles to the gas is shown in the figure to continuously decrease. This trend can be attributed to the reduction in gas density through the nozzle, and the far more rapid reduction in gas density within the plume. This density effect outweighs the influence of the growing temperature lag, so that even as the average energy transferred per interphase collision increases with downstream distance, the decline in collision frequency results in an overall reduction in the heat transfer rate as particles move downstream. Because the

drop-off in gas density is most prominent in the near-field region of the plume, the decrease in the heat transfer rate should be greatest in this region just beyond the nozzle exit, as is shown in Fig. 13.

The average heat transfer rate to the particle phase can be expressed as $\dot{Q}_p = M_p c_s \mathbf{u}_p \cdot \nabla T_p$, where M_p is the particle mass, c_s is the particle specific heat, $\mathbf{u}_p$ is the mean particle velocity, and T_p is the average temperature of the particles. The gradient of T_p should then scale roughly with the magnitude of the heat transfer rate. This trend is observed for all three simulations through a comparison of Fig. 13 with Fig. 14, which shows the variation of average particle temperature with distance along the axis. As displayed in Fig. 14, the particle temperature varies significantly through the nozzle and the near-field plume region, then reaches a nearly constant value within a short distance of the nozzle exit. This final value is found to be highly dependent on the gas source pressure. Note that analogous trends for the particle speed are observed in Fig. 10.

As shown in Equation 2, the force exerted on a particle by a colliding gas molecule will depend on the temperature of the particle. It follows that a change in particle temperature must alter the magnitude of the average force on the particles, so that the distribution of particle speed will also change. Figure 15 shows the ratio of the cell-averaged particle speed c_p in all three simulations to the particle speed c_p^o at the same locations, in the corresponding simulations where the inflow particle temperature is set to the original value of 298 K. This ratio (c_p/c_p^o) is plotted over 100 points along the central axis.

From Equation 2, it is expected that an increase in particle temperature will result in a greater force exerted on the particles by the accelerating gas. As T_p increases, values of c_p should then increase, and the ratio (c_p/c_p^o) should be greater than one. This is observed in Fig. 15, where (with the exception of a very few points near the inflow boundary which are not shown, and where c_p/c_p^o is just slightly below unity) the ratio of particle speeds is found to be consistently greater than one. In addition, the values of (c_p/c_p^o) tend to rise with downstream distance, because the force – and therefore the spatial gradient in the particle speed – will increase with particle temperature. The considerable statistical scatter observed in Fig. 15 is a consequence of the fact that even though the particle speed is influenced by the value of T_p, this influence is relatively small, and the ratio (c_p/c_p^o) is consistently very close to unity.

CONCLUSIONS AND FUTURE WORK

The method of Gallis et al.[4] has been fully implemented in a general DSMC code with capabilities for two dimensional or axisymmetric simulations of rarefied two phase flows, and initial validation of this code has been performed through comparison with experimental results. Due to a lack of experimental data usable for direct quantitative comparison, much of the validation method employed is inherently qualitative. However, numerical results do agree well with results from the experiment. It can then be concluded that, in general, both the method and implementation are relatively accurate for the flow regimes considered.

The ultimate goal of this project is the development of a general simulation method for modeling two phase plumes from high-altitude rockets and spacecraft thrusters. Several major additions to the code are therefore either planned or in progress, in order to improve on the accuracy, efficiency, or applicability of the code. As discussed above, a new method is being developed for the general simulation of two-way coupled two phase flows. Other modifications in progress include the consideration of nonspherical particles, combusting or chemically reactive particles, and the automatic characterization of the flow in each grid cell as either uncoupled, one-way coupled, or two-way coupled in order to neglect unnecessary calculations and improve computational efficiency. These modifications are expected to be discussed in a future paper[11].

Further planned modifications include the modeling of finite-rate particle phase change (between liquid and solid states) and interphase mass transfer, as well as particle breakup, agglomeration, and cluster formation. Likely the most extensive future addition will be a radiation model, which will include effects of radiative heat transfer within the particle phase, as well as between particles and the ambient surroundings or any solid boundaries.

ACKNOWLEDGMENTS

The authors gratefully acknowledge the financial support for this work provided by the Air Force Research Laboratory at Edwards Air Force Base, with Jay Levine as technical monitor.

REFERENCES

1. York, B. J., Lee, R. A., Sinha, N., and Dash, S. M., "Progress in the Simulation of Particulate Interactions in Solid Propellant Rocket Exhausts," AIAA Paper 2001-3590, July 2001.
2. Dash, S. M., Wolf, D. E., Beddini, R. A., and Pergament, H. S., "Analysis of Two-Phase Flow Processes in Rocket Exhaust Plumes," *Journal of Spacecraft and Rockets*, Vol. 22, No. 3, 1985, pp. 367-380.
3. Bird, G. A., *Molecular Gas Dynamics and the Direct Simulation of Gas Flows*, Clarendon Press, Oxford, 1994, pp. 203-220.

4. Gallis, M. A., Torczynski, J. R., and Rader, D. J., "An Approach for Simulating the Transport of Spherical Particles in a Rarefied Gas Flow via the Direct Simulation Monte Carlo Method," *Physics of Fluids*, Vol. 13, No. 11, 2001, pp. 3482-3492.
5. Dietrich, S., and Boyd, I. D., "Scalar and Parallel Optimized Implementation of the Direct Simulation Monte Carlo Method," *Journal of Computational Physics*, Vol. 126, 1996, pp. 328-342.
6. Crowe, C., Sommerfeld, M., and Tsuji, Y., *Multiphase Flows with Droplets and Particles*, CRC Press, New York, 1998, pp. 43 50, 113-121.
7. Chen, X.-Q., "Efficient Particle Tracking Algorithm for Two-Phase Flows in Geometries using Curvilinear Coordinates," *Numerical Heat Transfer*, Part A, Vol. 32, Taylor and Francis, 1997, pp. 387-405.
8. Epstein, P. S., "On the Resistance Experienced by Spheres in their Motion through Gases," *Physical Review*, Vol. 24, 1924, pp. 710-733.
9. Moylan, B., and Sulyma, P., "Investigation of Gas/Particle Heat Transfer Rates in Solid Rocket Motors," AIAA Paper 92-3619, July 1992.
10. Israel, G., and Friedlander, K., "High-Speed Beams of Small Particles," *Journal of Colloid and Interface Science*, Vol. 24, 1967, pp. 330-337.
11. Burt, J. M., and Boyd, I. D., "Development of a Two-Way Coupled Model for Two Phase Rarefied Plume Flows," to be presented at 42nd AIAA Aerospace Sciences Meeting in Reno, NV, Jan. 2004.
12. Hill, J. A. F., and Draper, J. S., "Analytical Approximation for the Flow from a Nozzle into a Vacuum," *Journal of Spacecraft*, Vol. 3, No. 10, 1966, pp. 1552-1554.

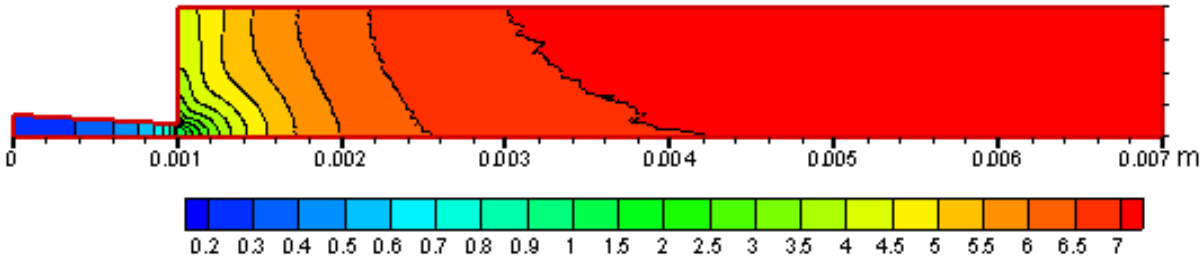

Figure 1. Contours of gas Mach number for a source pressure of 34.5 mmHg.

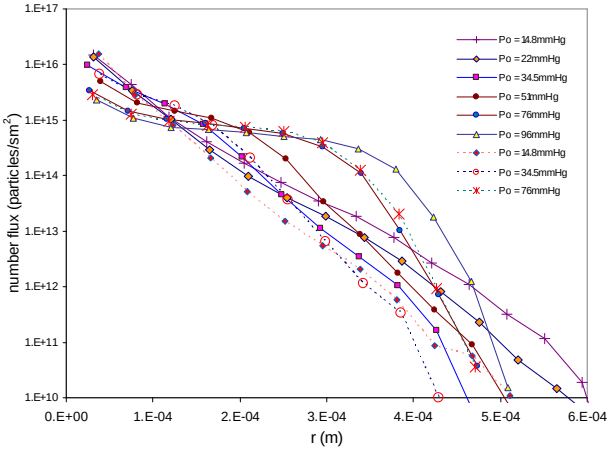

Figure 2. Particle number flux profiles along outflow boundary. Dotted lines correspond to simulations where inflow particle velocity varies with distance from the axis.

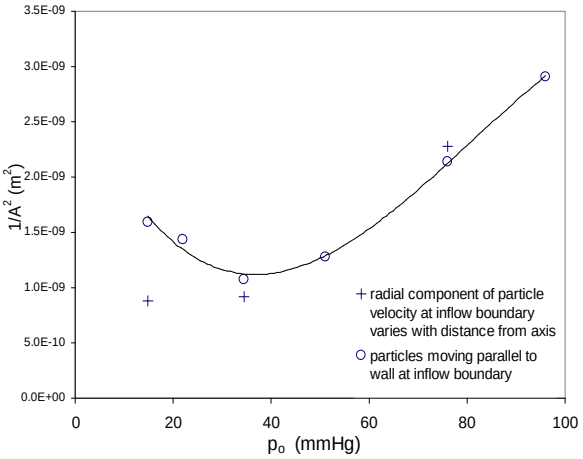

Figure 3. Values of $1/A^2$ as a function of source pressure, based on the numerical results.

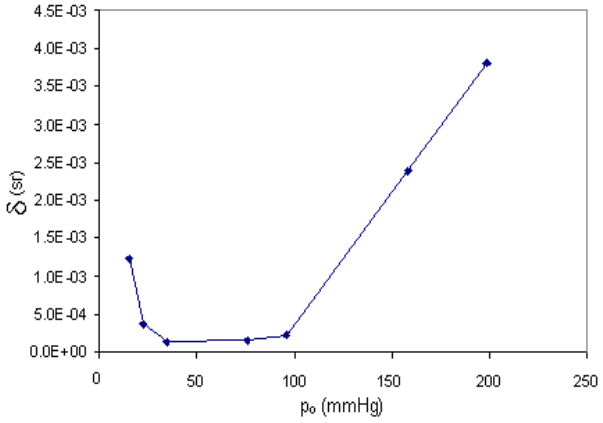

Figure 4. Source pressure vs. experimental values of δ.

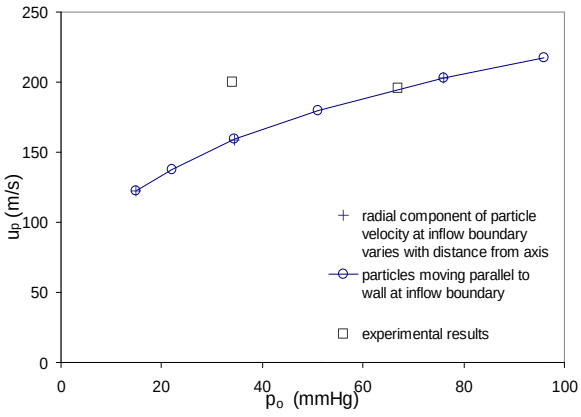

Figure 5. Variation with source pressure of terminal particle velocity along the central axis.

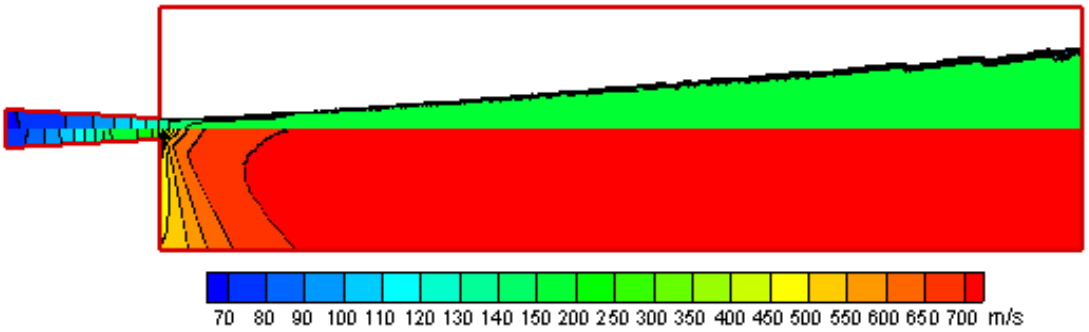

Figure 6. Magnitudes of particle and gas velocity.

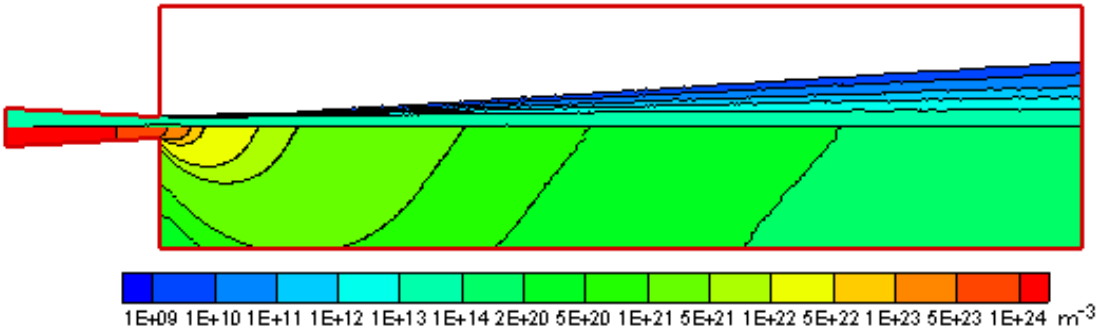

Figure 7. Contours of particle and gas number densities.

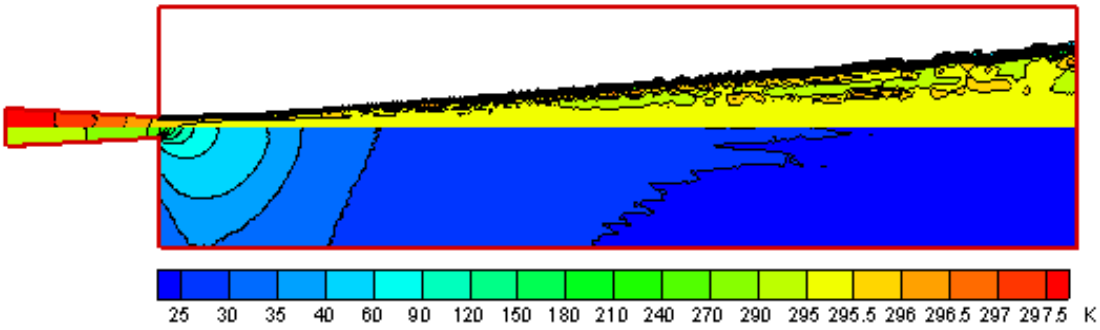

Figure 8. Contours of average particle temperature and gas translational temperature.

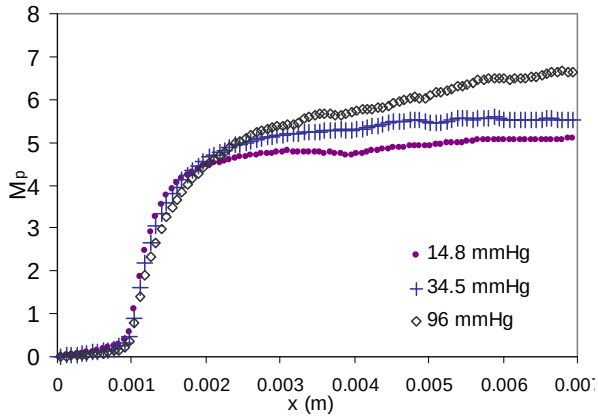

Figure 9. Comparison of relative particle Mach numbers along the central axis for simulations at three different source pressures.

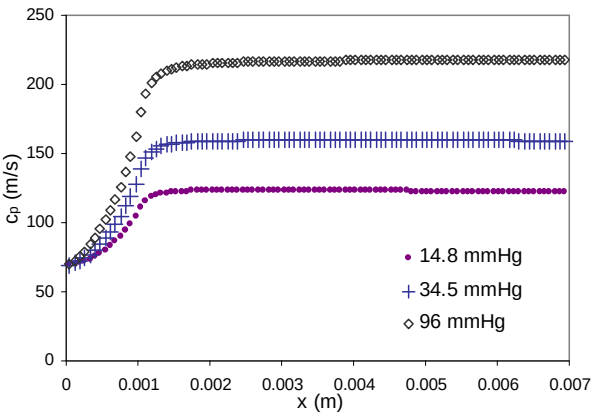

Figure 10. Particle speed along the central axis.

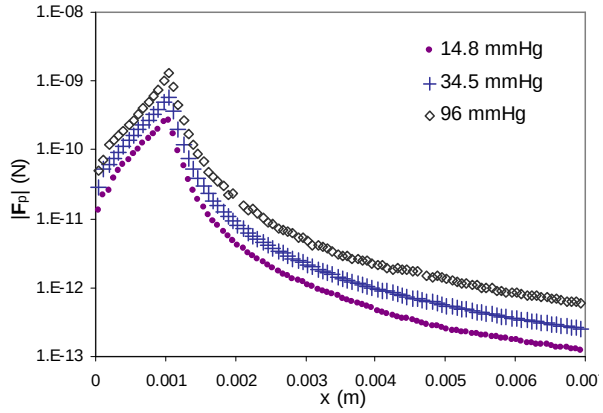

Figure 11. Drag force on particles along the central axis.

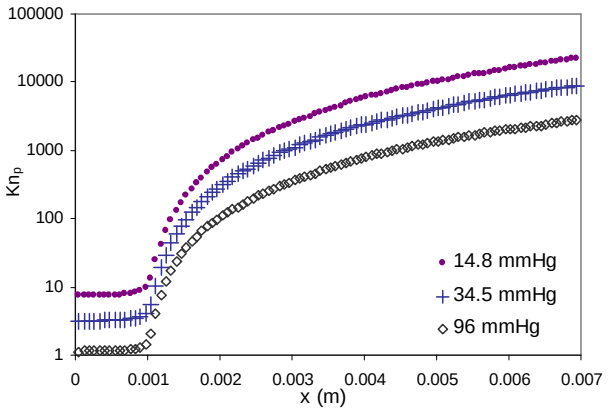

Figure 12. Particle Knudsen number along the central axis.

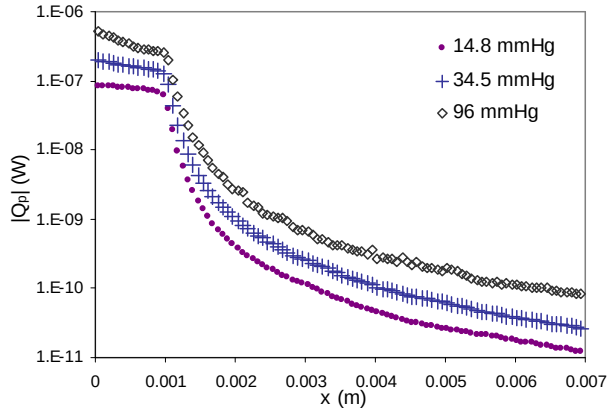

Figure 13. Magnitude of the average particle heat transfer rate along the central axis.

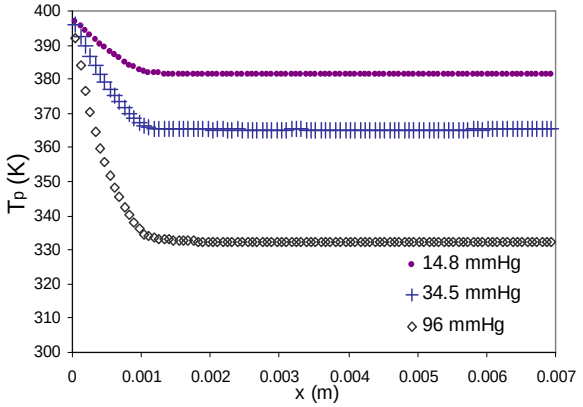

Figure 14. Average particle temperature along the axis.

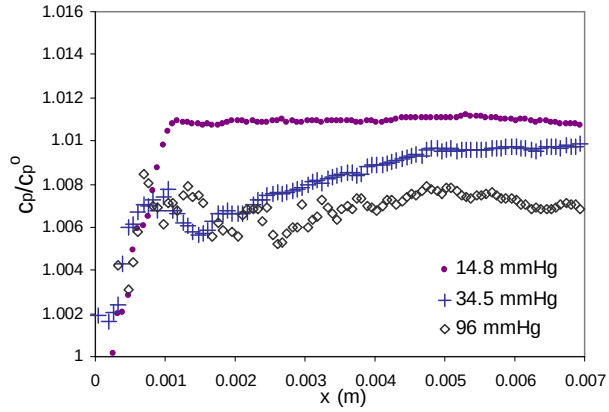

Figure 15. Fractional change in average particle speed due to an increase in particle temperature.